Electronic Supplementary Information

A heterostructure of NiMn LDH nanosheets assembled on ZIF-L-derived ZnCoS hollow nanosheets with built-in electric field enables boosted electrochemical energy storage

Tong Li,[a, ⊥] Xuanying Hu,[a, ⊥] Cui Yang,[b*] Lei Han,[a] and Kai Tao[a*]

[a] School of Materials Science & Chemical Engineering, Ningbo University, Ningbo, Zhejiang 315211, P. R. China.

[b] Institute of Drug Discovery Technology, Ningbo University, Ningbo, Zhejiang, 315211, P. R. China; Email: yangcui@nbu.edu.cn

E-mails: taokai@nbu.edu.cn, yangcui@nbu.edu.cn

⊥ These authors contributed equally to this work.

Characterization

The microstructure and composition of the prepared samples were characterized by field emission scanning electron microscopy (FESEM, Hitachi S-4800) and transmission electron microscopy (TEM, FEI Tecnai F30) equipped with selected area electron diffraction (SAED) and energy dispersive X-ray spectroscopy (EDS). Crystalline phase and structural analyses were performed by X-ray diffractometer (XRD, Bruker AXS D8 Advance). X-ray photoelectron Spectroscopy (XPS, Thermo Scientific K-Alpha) was used to characterize the elemental compositions and

chemical states. Fourier transform infrared spectroscopy (FTIR) was performed using a NICOLET-5700 FTIR spectrometer in the wave number range of 400 to 4000 cm^{-1}. An ultraviolet photoelectron spectrometer (UPS, PHI5000 VersaProbe III) was used to determine the work function and valence band of the sample. The bandgap of the sample was analyzed by the ultraviolet-visible diffuse reflectance spectrum (UV-vis DRS, LAMBDA 850+).

Electrochemical measurements

Electrochemical measurements including cyclic voltammetry (CV), constant current charge and discharge (GCD) and electrochemical impedance spectroscopy (EIS) were carried out on a CHI660E electrochemical workstation (Shanghai Shenhua). All tests were carried out at ambient temperature in an aqueous solution containing KOH (2 M). The electrochemical performance of the prepared integrated electrodes was evaluated in a three-electrode system, where the prepared electrode (1×1 cm^2), saturated calomel electrode (SCE) and platinum foil were used as working, reference, and counter electrodes, respectively. The specific capacitance (C, F g^{-1}) was calculated from the GCD curve using the following equation:

$$C = \frac{I \times \Delta t}{m \times \Delta V} \quad (1)$$

where I (A), $\Delta t\ (t)$, m (g) and $\Delta V\ (V)$ represent the discharge current, discharge time, mass of active materials and discharge potential, respectively.

The charge storage mechanism was analyzed by the following equation:

$$i = a\upsilon^{b} \quad (S2)$$

where i (A) and υ (mV s^{-1}) represent peak current and scan rate, constant and constant, respectively. a and b are constants. When b=0.5, the charge storage is regarded as diffusion-controlled while the storage mechanism is considered as capacitive if b=1. The capacitive ($k_1\upsilon$) and diffusion-controlled ($k_2\upsilon^{1/2}$) contributions to the total current response were separated by the following equation:

$$i(V) = k_1\upsilon + k_2\upsilon^{1/2} \quad (S3)$$

A two-electrode asymmetric supercapacitor (ASC) was constructed from the prepared ZCS@LDH-6 (cathode) and an activated carbon (AC) electrode (anode). The AC electrode was prepared using a standard slurry casting method. The slurry was made from a mixture of AC, conductive agent (acetylene black) and polyvinylidene fluoride (PVDF) binder in 1-methyl-2-pyrrolidone (NMP) solvent with a mass ratio of 8:1:1. The slurry was then coated onto nickel foam (1 cm×1 cm), dried and finally pressed. The mass loading of the active material was kept at 1~2 mg/cm^2. To obtain better energy storage performance, charge balance between the two electrodes was achieved by adjusting the mass ratio of the cathode to anode by following equation:

$$\frac{m_+}{m_-} = \frac{C_- \times \Delta V_-}{C_+ \times \Delta V_+}$$

where m (g), C (F g^{-1}) and ΔV (V) represent mass of active materials, specific

capacitance and discharging potential of positive and negative electrodes, respectively. Energy density (E, Wh kg^{-1}) and power density (W kg^{-1}) of the ZCS@LDH-6//AC ASC device were calculated by using the following equations:

$$E = \frac{C \times (\Delta V)^2}{2 \times 3.6} \quad (5)$$

$$P = \frac{3600E}{\Delta t} \quad (6)$$

where C (F g^{-1}), Δt (s) and ΔV (V) represent specific capacitance, discharging time and working voltage of ZCS@LDH-6//AC cell, respectively.

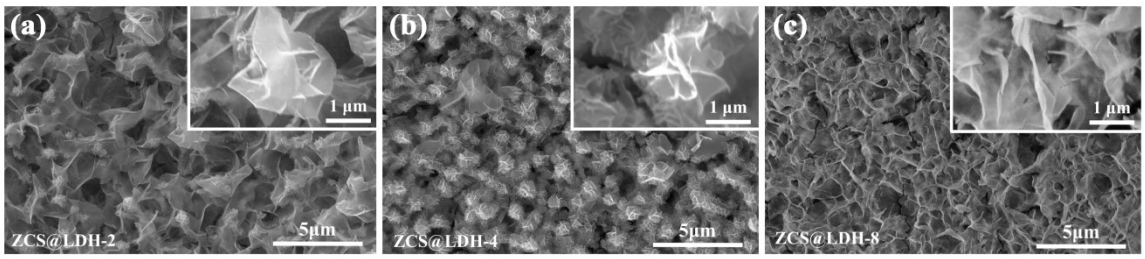

Figure S1. SEM images of (a) ZCS@LDH-2, (b) ZCS@LDH-4, and (c) ZCS@LDH-8.

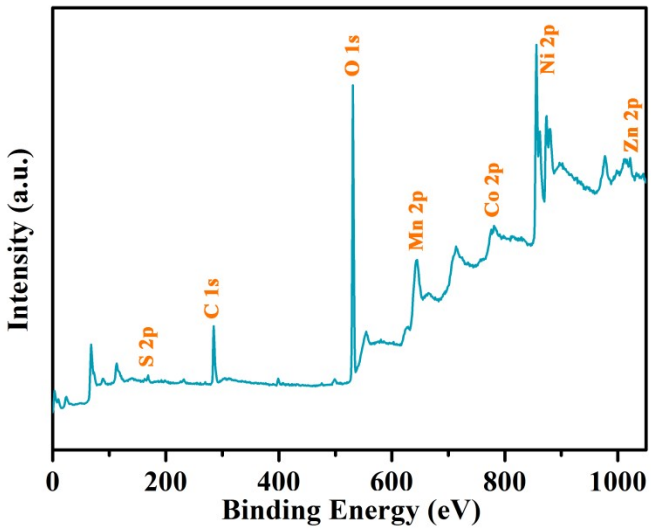

Figure S2. XPS scan spectrum of the ZCS@LDH-6.

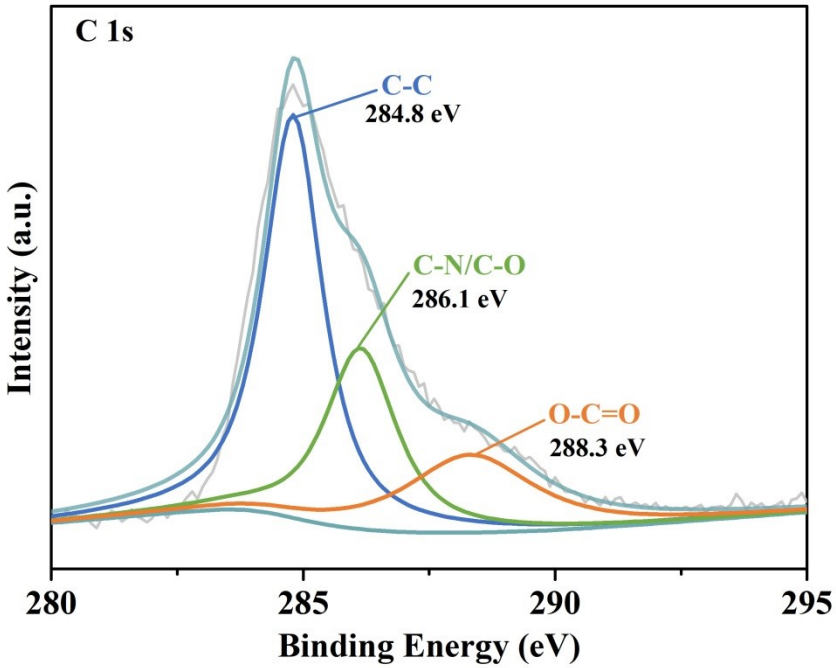

Figure S3. High-resolution C 1s spectrum of ZCS@LDH-6.

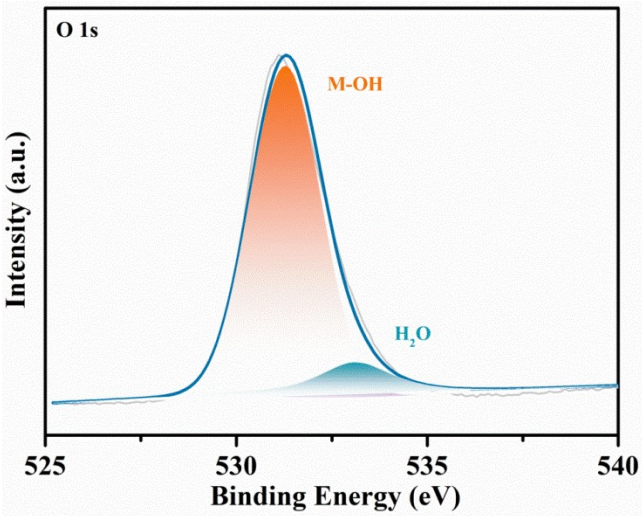

Figure S4. High-resolution O 1s spectrum of ZCS@LDH-6.

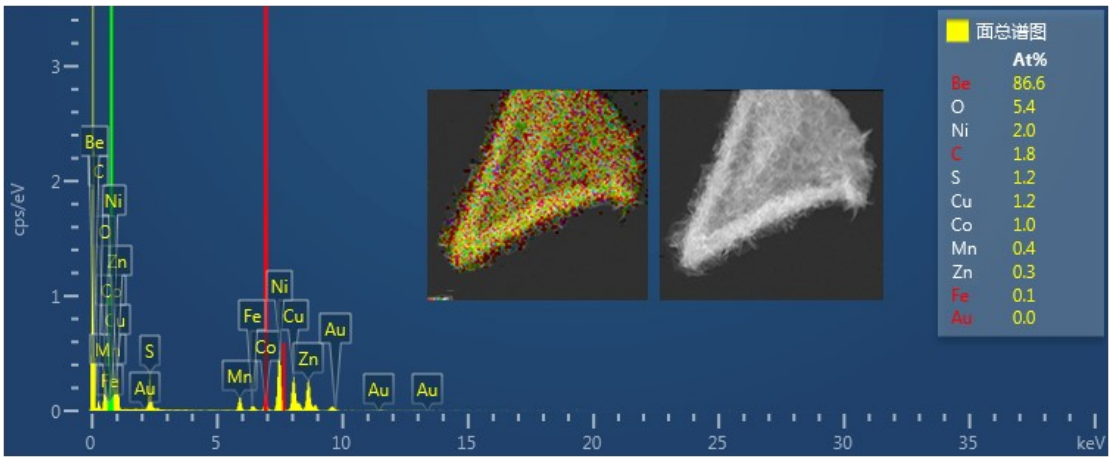

Figure S5. EDS pattern of the ZCS@LDH-6.

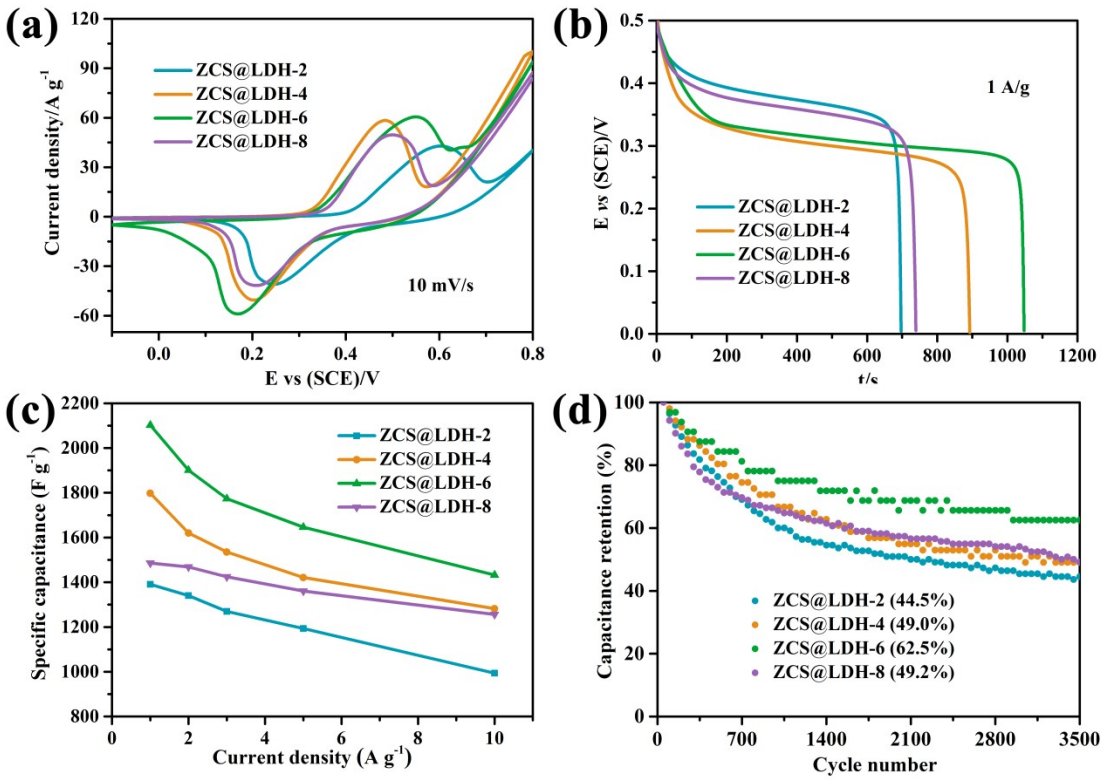

Figure S6. Comparison of (a) CV, (b) GCD, (c) specific capacitance and (d) cycling stability of the ZCS@LDH-2, ZCS@LDH-4, ZCS@LDH-6 and ZCS@LDH-8.

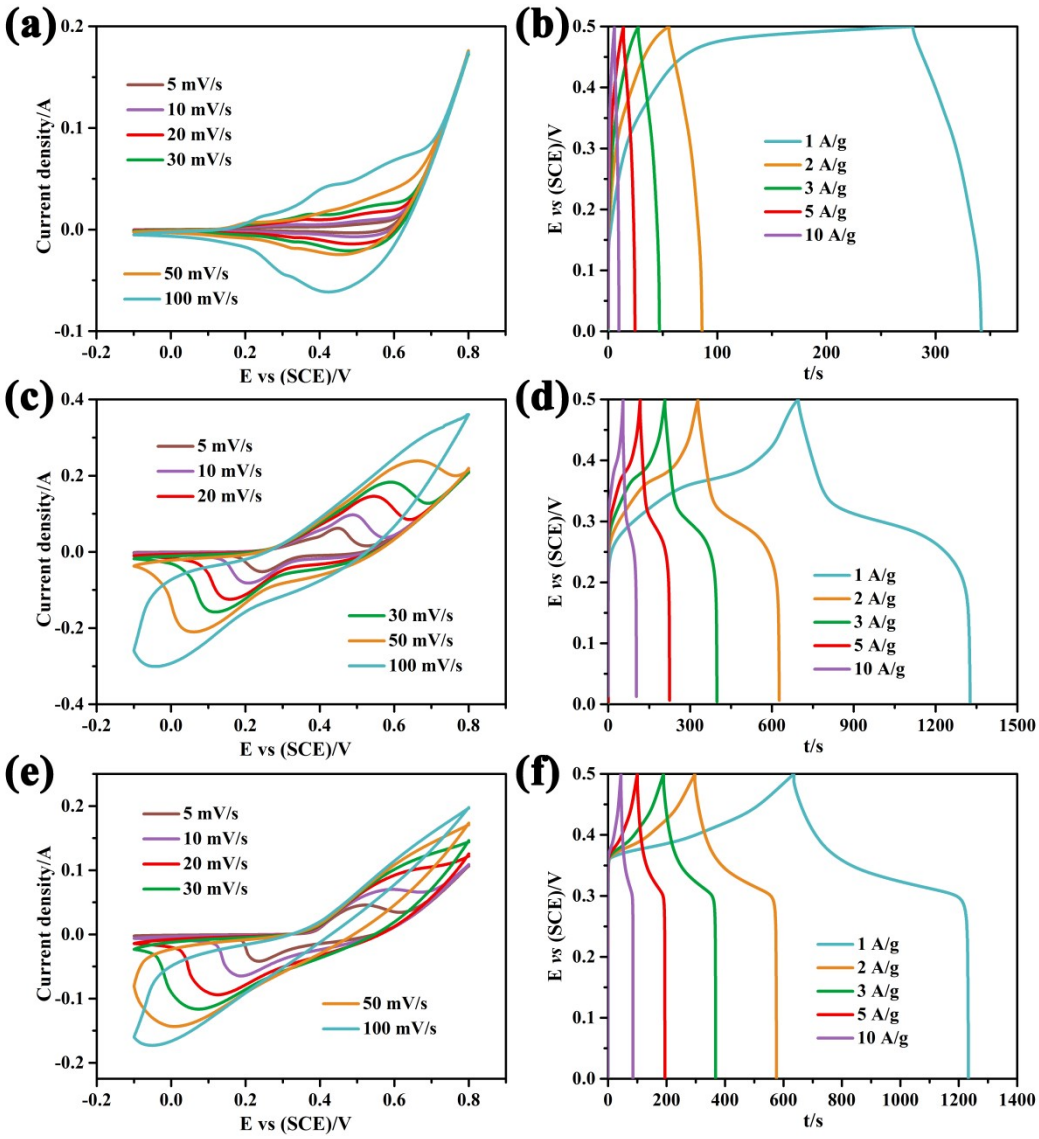

Figure S7. (a, c, e) CV and (b, d, f) GCD curves of (a, b) ZnCo-ZIF/NF, (c, d) ZnCoS/NF and (e, f) NiMn-LDH/NF.

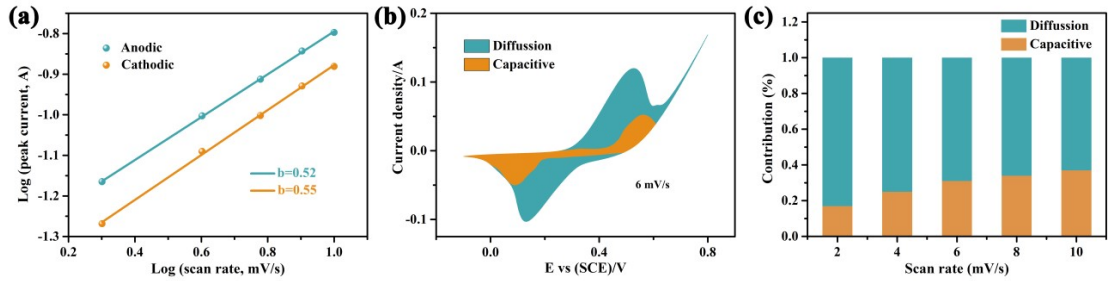

Figure S8. Analysis of charge storage mechanism of the ZCS@LDH-6 electrode. (a) Log (*i*) *vs.* Log (*v*). (b) CV curve showing the contributions of capacitive and diffusion-controlled processes at 6 mV s^{-1}. (c) The contribution fractions of the capacitive and diffusion-controlled processes at 2-10 mV s^{-1}.

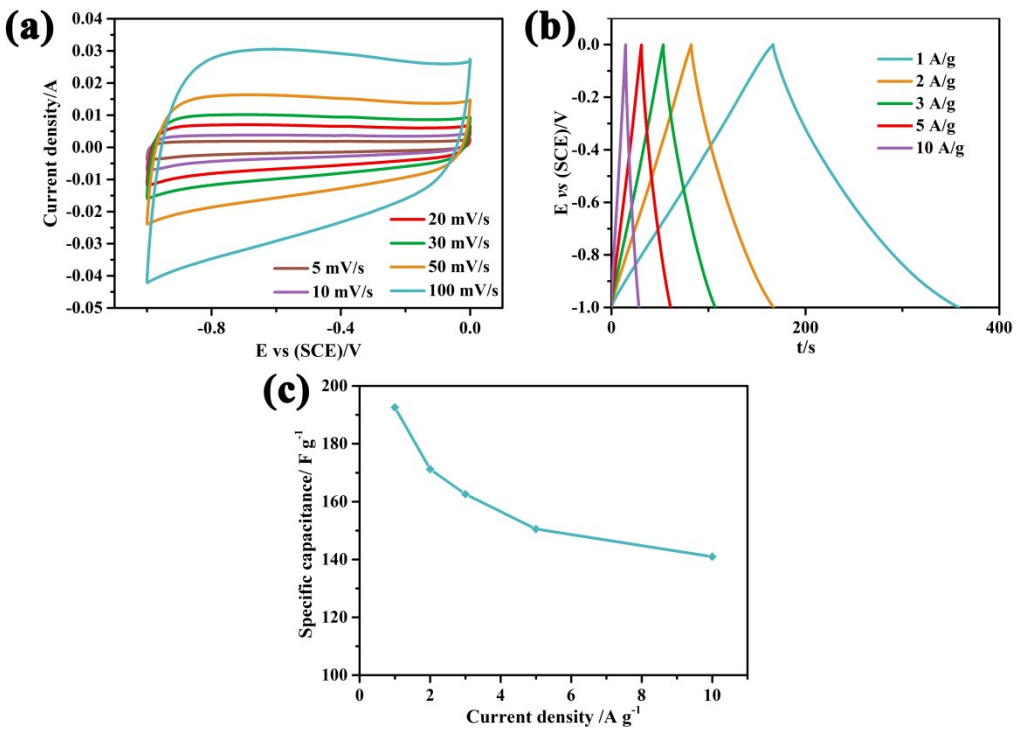

Figure S9. (a) CV curves at various scan rates, (b) GCD curves at different current densities and (c) Specific capacitances of AC.

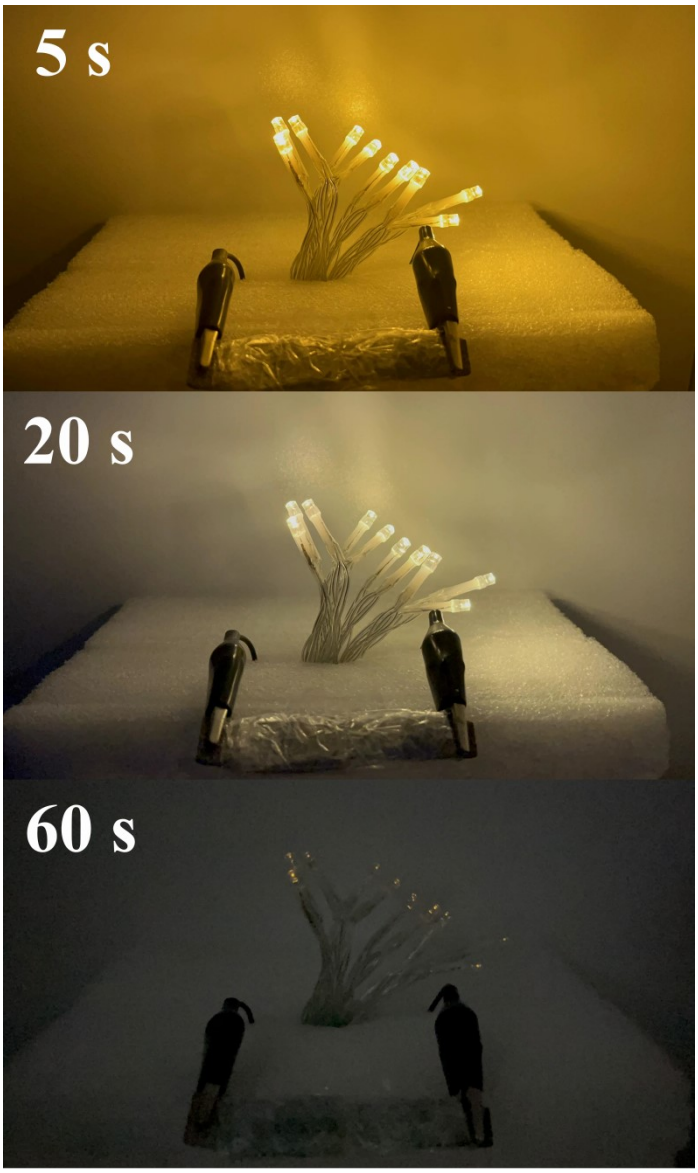

Figure S10. Photographs of the lighted LEDs powered by two assembled ZCS@LDH-6//AC ASCs.

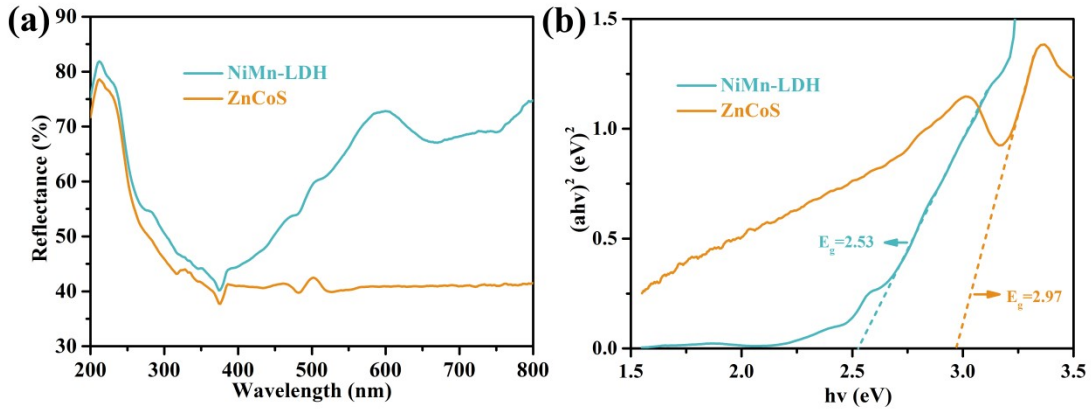

Figure S11. (a) UV-vis diffusive reflectance spectra and (b) Tauc-Mott plots of ZnCoS and NiMn-LDH.

Table S1. EIS results of the ZnCo-ZIF, ZnCoS, NiMn-LDH and ZCS@LDH-6

Electrode	ZnCo-ZIF	ZnCoS	NiMn-LDH	ZCS@LDH-6
R_s (Ω)	1.15	0.89	0.69	0.61
R_{ct} (Ω)	1.18	0.73	1.41	0.49

Table S2. Comparison of specific capacitance with previous studies.

electrode materials	current density	specific capacitance	reference
ZCS@LDH-6	1 A g^{-1}	2102.2 F g^{-1}	this work
ZnCoS-rGO HMFs	1 A g^{-1}	1225.1 F g^{-1}	1
ZnCoS/C 20	1 A g^{-1}	682 C g^{-1}	2
Ni-Mn LDH/CNTs/rGO	1 A g^{-1}	1268 F g^{-1}	3
LNCF-2	0.5 A g^{-1}	2128.3 F g^{-1}	4
NiMn-LDH/hrGO	1 A g^{-1}	302.0 C g^{-1}	5
Zn-Co-S	1 A g^{-1}	1646 F g^{-1}	6
ZCS@ZCNS-2	0.5 A g^{-1}	1603 F g^{-1}	7

Table S3. Comparison of the energy storage capability of this work with literature.

ASC	energy density	power density	reference
ZCS@LDH-6//AC	41.7 Wh kg^{-1}	850 W kg^{-1}	this work
ZnCoS//PrGO	17.7 Wh kg^{-1}	435 W kg^{-1}	8
Zn-Co-S/NF//AC/NF	31.9 Wh kg^{-1}	850 W kg^{-1}	9
$ZnCo_2S_4$@PPy//AC	33.78 Wh kg^{-1}	800.05 W kg^{-1}	10
ZnCoS/C 20//PrGO	40.6 Wh kg^{-1}	762 W kg^{-1}	2
LNCF-2//NCF	34.1 Wh kg^{-1}	350.1 W kg^{-1}	4
rGO@NiMn-LDH@NF//AC	22.5 Wh kg^{-1}	700 W kg^{-1}	11
NiMn-LDH@MWCNT//AC	11.86 Wh kg^{-1}	3707.77 W kg^{-1}	12

References

1. Chen, P.; Yang, C.; Gao, P.; Chen, X.; Cheng, Y.-J.; Liu, J.; Guo, K., Distinctive Formation of Bifunctional ZnCoS-rGO 3D Hollow Microsphere Flowers with Excellent Energy Storage Performances. *Chemistry of Materials* **2022,** *34* (13), 5896-5911.
2. YuanZhang; HuiWang, Epitaxial ZnCoS nanodendritics grown along 3-D carbonaceous scaffolds for high-performance hybrid supercapacitors. *Journal of Alloys and Compounds* **2022,** *905*, 164250.
3. Li, M.; Liu, F.; Zhang, X. B.; Cheng, J. P., A comparative study of Ni-Mn layered double hydroxide/carbon composites with different morphologies for supercapacitors. *Physical Chemistry Chemical Physics* **2016,** *18* (43), 30068-30078.
4. Chen, D.; Yan, S.; Chen, H.; Yao, L.; Wei, W.; Lin, H.; Han, S., Hierarchical Ni–Mn layered double hydroxide grown on nitrogen-doped carbon foams as high-performance supercapacitor electrode. *Electrochimica Acta* **2018,** *292*, 374-382.
5. Yan, W.; Zhang, Y.; Zeng, T.; Zhang, Y.; Wan, Q.; Yang, N., A high-performance asymmetric supercapacitor using composite electrodes of layered double hydroxides and holey reduced graphene oxide. *Journal of Energy Storage* **2022,** *52*, 104899.
6. Chameh, B.; Moradi, M.; Kaveian, S., Synthesis of hybrid ZIF-derived binary ZnS/CoS composite as high areal-capacitance supercapacitor. *Synthetic Metals* **2020,** *260*, 116262.
7. Jia, H.; Fan, J.; Fan, Y.; Feng, C.; Jin, H.; Cai, Y.; Liu, M.-C., Cation substituted Ni3S2 nanosheets wrapped Zn0.76Co0.24S nanowire arrays prepared with in-situ oxidative etching strategy for high performance solid-state asymmetric supercapacitors. *Journal of Energy Storage* **2022,** *46*, 103870.
8. Zhang, Y.; Cao, N.; Szunerits, S.; Addad, A.; Roussel, P.; Boukherroub, R., Fabrication of ZnCoS nanomaterial for high energy flexible asymmetric supercapacitors. *Chem. Eng. J.* **2019,** *374*, 347-358.
9. Tao, K.; Han, X.; Cheng, Q.; Yang, Y.; Yang, Z.; Ma, Q.; Han, L., A Zinc Cobalt Sulfide Nanosheet Array Derived from a 2D Bimetallic Metal-Organic Frameworks for High-Performance Supercapacitors. *Chemistry* **2018,** *24* (48), 12584-12591.
10. Wang, X.; Wang, Y.; Jiang, Y.; Li, X.; Liu, Y.; Xiao, H.; Ma, Y.; Huang, Y. y.; Yuan, G., Tailoring Ultrahigh Energy Density and Stable Dendrite‐Free Flexible Anode with Ti3C2Tx MXene Nanosheets and Hydrated Ammonium Vanadate Nanobelts for Aqueous Rocking‐Chair Zinc Ion Batteries. *Adv. Funct. Mater.* **2021,** *31* (35), 2103210.
11. Sun, L.; Zhang, Y.; Zhang, Y.; Si, H.; Qina, W.; Zhang, Y., Reduced Graphene Oxide Nanosheet Modified NiMn-LDH nanoflake arrays for High-Performance Supercapacitors *Chemical Communications* **2018,** *54* (72), 10172-10175.
12. Li, Y.; Hu, B.; Hu, B.; Xu, C.; Yang, S.; Yu, J.; Zhang, B.; Liu, Y.; Yu, D.; Chen, C., In Situ Fabrication of NiMn‐LDH@MWCNT Composites with Hierarchical Structure for Superior Electrochemical Energy Storage. *ChemElectroChem* **2021,** *8* (17), 3339-3347.